International Journal of Fracture **53**: 273–289, 1992.

Bifurcation and stability of structures with interacting propagating cracks

ZDENĚK P. BAŽANT and MAZEN R. TABBARA
Department of Civil Engineering and Center for Advanced Cement-Based Materials, Northwestern University, Evanston, Illinois 60208, USA

Received 15 June 1990; accepted 15 April 1991

Abstract. A general method to calculate the tangential stiffness matrix of a structure with a system of interacting propagating cracks is presented. With the help of this matrix, the conditions of bifurcation, stability of state and stability of post-bifurcation path are formulated and the need to distinguish between stability of state and stability path is emphasized. The formulation is applied to symmetric bodies with interacting cracks and to a halfspace with parallel equidistant cooling cracks or shrinkage cracks. As examples, specimens with two interacting crack tips are solved numerically. It is found that in all the specimens that exhibit a softening load-displacement diagram and have a constant fracture toughness, the response path corresponding to symmetric propagation of both cracks is unstable and the propagation tends to localize into a single crack tip. This is also true for hardening response if the fracture toughness increases as described by an R-curve. For hardening response and constant fracture toughness, on the other hand, the response path with both cracks propagating symmetrically is stable up to a certain critical crack length, after which snapback occurs. A system of parallel cooling cracks in a halfspace is found to exhibit a bifurcation similar to that in plastic column buckling.

1. Introduction

The study of structures containing many cracks is important for the understanding of damage and failure processes. One difficult aspect of crack systems is that there exist bifurcations and multiple post-bifurcation paths. This is due to the fact that for the same loading one can find different solutions, with different crack lengths. Determination of such bifurcations and identification of the correct post-bifurcation path is a problem of stability theory of structures with irreversible deformations. While the theory of bifurcation in plastic buckling of columns has been developed long ago, the general problem of stability analysis of structures with irreversible deformations due to plasticity, damage or cracking has not been successfully tackled until recently, although various relevant stability conditions have been introduced as postulates, without thermodynamic foundations; see Meier [1], Bažant [2], Petryk [3], Nguyen and Stolz [4], Nguyen [5] and Stolz [6], who extended Hill's [7] bifurcation and uniqueness concepts for plasticity. In this paper a recently formulated general method [8] of stability analysis of inelastic structures will be applied to elastic structures with propagating interacting cracks. Bifurcations and stability in symmetric structures with a pair of symmetric initial cracks, and in a half-space with a system of parallel equidistant shrinkage or cooling cracks in a halfspace will be analyzed.

2. Structures with interacting growing cracks

First we need to briefly describe the general method of stability analysis of elastic structures with growing interacting cracks. Consider a structure whose state is characterized by the

displacement vector $\boldsymbol{q} = (q_1, \ldots, q_N)^T$ and the crack length vector $\boldsymbol{a} = (a_1, \ldots, a_M)^T$. For equilibrium (non-dynamic) crack propagation, we have:

$$\frac{\partial \Pi}{\partial a_k} + R_k = 0, \tag{1}$$

where R_k = given R-curve of the kth crack, $\Pi = \Pi(\boldsymbol{q}, \boldsymbol{a}) = U - W$ = potential energy of the structure; U = strain energy, and W = work of applied loads.

Consider now crack length increments δa_r such that the cracks $r = 1, \ldots, m$ remain propagating while cracks $m + 1$ to M stop propagating. The condition of continuing propagation of cracks a_r is $\delta(\partial \Pi / \partial a_k + R_k) = 0$ with $k = 1, \ldots, m$; therefore, differentiating (1) and setting $\delta R_k = R' \delta a_k$ we obtain

$$\sum_{r=1}^{m} \frac{\partial}{\partial a_r} \frac{\partial \Pi}{\partial a_k} \delta a_r + \sum_{j=1}^{N} \frac{\partial}{\partial q_j} \frac{\partial \Pi}{\partial a_k} \delta q_j + R' \delta a_k = 0. \tag{2}$$

Introducing the matrix

$$\Phi_{rk} = \frac{\partial^2 \Pi}{\partial a_r \partial a_k} + R' \delta_{rk}, \tag{3}$$

where δ_{rk} = Kronecker delta, we can write (2) in the form

$$\sum_{r=1}^{m} \Phi_{rk} \delta a_r + \sum_{j=1}^{N} \frac{\partial^2 \Pi}{\partial q_j \partial a_k} \delta q_j = 0. \tag{4}$$

If matrix $[\Phi_{rk}]$ is not singular, we can obtain the inverse matrix

$$[\Psi_{rk}] = [\Phi_{rk}]^{-1}. \tag{5}$$

Equation (4) may then be solved for δa_r

$$\delta a_r = -\sum_{k=1}^{m} \Psi_{rk} \sum_{j=1}^{N} \frac{\partial^2 \Pi}{\partial q_j \partial a_k} \delta q_j. \tag{6}$$

Consider now that displacements q_j ($j = 1, \ldots, N$) vary at the same time as the cracks extend by δa_r ($r = 1, \ldots, m$). Then the equilibrium force variations δf_i ($i = 1, \ldots, N$) associated with δq_j are given by

$$\delta f_i = \sum_{j=1}^{N} \frac{\partial f_i}{\partial q_j} \delta q_j + \sum_{r=1}^{m} \frac{\partial f_i}{\partial a_r} \delta a_r = \sum_{j=1}^{N} S_{ij}^{s} \delta q_j + \sum_{r=1}^{m} \frac{\partial^2 \Pi}{\partial a_r \partial q_i} \delta a_r \tag{7}$$

in which $S_{ij}^{s} = \partial^2 \Pi / \partial q_i \partial q_j$ = secant stiffness matrix of the structure = elastic stiffness matrix at stationary cracks. Substituting (6) for δa_r, we acquire an equation that can be put into the form

$$\delta f_i = \sum_{j=1}^{N} S_{ij}^{t} \delta q_j \tag{8}$$

in which

$$S_{ij}^t = S_{ij}^s - \sum_{k=1}^{m} \sum_{r=1}^{m} \Psi_{rk} \frac{\partial^2 \Pi}{\partial a_r \partial q_i} \frac{\partial^2 \Pi}{\partial q_j \partial a_k}. \tag{9}$$

This is the tangential stiffness matrix of a structure with propagating cracks. As we see, it is symmetric. The second-order work done on the displacement variations is

$$\delta^2 W = \frac{1}{2} \sum_{i=1}^{N} \sum_{j-1}^{N} S_{ij}^t \delta q_i \delta q_j. \tag{10}$$

This expression gives admissible values provided that two conditions are met: (1) $\delta a_r \geqslant 0$ for $r = 1, \ldots, m$ and (2) $\delta(\partial \Pi / \partial a_s + R_s) < 0$ for $s = m + 1, \ldots, M$.

As shown by thermodynamic analysis [8, 22], the structure is stable if $\delta^2 W > 0$ for all admissible (equilibrium or nonequilibrium) variations, unstable if $\delta^2 W < 0$ for some admissible variations, and critical if $\delta^2 W = 0$. Moreover, when bifurcation occurs and the states on all equilibrium paths are stable, the equilibrium path that is followed after bifurcation is that for which $\delta^2 W$ is minimum.

Let us now analyze path bifurcation, choosing as δq_j only those displacements that are controlled. This means that the displacements associated with prescribed forces may be used in calculating Π but are not included among the set of kinematic variables. Then δq_j have the same values for the post-bifurcation paths 1 and 2 while the crack length increments may have different values, $\delta a_r^{(1)}$ for path 1 and $\delta a_r^{(2)}$ for path 2. Writing (4) for these two paths, we obtain

$$\sum_{r=1}^{m} \Phi_{rk} \delta a_r^{(1)} + \sum_{j=1}^{N} \frac{\partial^2 \Pi}{\partial a_k \partial q_j} \delta q_j = 0, \tag{11}$$

$$\sum_{r=1}^{m} \Phi_{rk} \delta a_r^{(2)} + \sum_{j=1}^{N} \frac{\partial^2 \Pi}{\partial a_k \partial q_j} \delta q_j = 0 \tag{12}$$

and subtracting these equations we obtain

$$\sum_{r=1}^{m} \Phi_{rk} \delta a_r^* = 0, \quad \text{where} \quad \delta a_r^* = \delta a_r^{(1)} - \delta a_r^{(2)}. \tag{13}$$

To satisfy (13), matrix $[\Phi_{rk}]$ must be singular, i.e. $\det[\Phi_{rk}] = 0$, or the lowest eigenvalue of $[\Phi_{rk}]$ must vanish. In calculating $[\Phi_{rk}]$, the derivatives $\partial^2 \Pi / \partial a_r \partial a_k$ must, of course, be evaluated for the case that the controlled displacements are kept constant, but other displacements associated with prescribed loads, possibly zero loads, can vary.

The foregoing solution is valid only if the values of Φ_{rk} and $\partial^2 \Pi / \partial a_k \partial q_j$ at the bifurcation point are the same for both paths 1 and 2. If the space of displacement increments is divided into sectors of:

1. all cracks $(1, \ldots, M)$ are growing,
2. $1, \ldots, m$ cracks are growing, while $m + 1, \ldots, M$ cracks are unloading and
3. all cracks $(1, \ldots, M)$ are unloading.

Then this condition means that both post-bifurcation paths must belong to the same sector of loading directions. This condition at first bifurcation is generally satisfied if the material properties vary continuously during the loading process, but is violated if they vary discontinuously (this is analogous to plastic buckling of columns with a bilinear stress-strain diagram). To see the reason why this is so, one needs to note that prior to the first bifurcation the eigenvector of matrix $[\Phi_{rk}]$ according to (13) lies in an inadmissible sector of loading directions, for which the conditions $\delta a_r \geqslant 0$ are not all satisfied; hence, there is no bifurcation. The direction of eigenvector δa_r^* gradually rotates and when it coincides with the boundary of the admissible sector of directions, the first bifurcation state is reached, i.e. different solutions $\delta a_r^{(1)}$ and $\delta a_r^{(2)}$ are for the first time possible. It follows that they both occur for the same Φ_{rk}.

On the other hand, when δa_r occur at constant displacements ($\delta q_j = 0$), for example due to temperature changes or shrinkage of the material, then the second order work is

$$\delta^2 W = \frac{1}{2} \sum_{r=1}^{m} \sum_{k=1}^{m} \Phi_{rk} \delta a_r \delta a_k. \tag{14}$$

3. Equilibrium paths for structures with two cracks

From now on we focus on symmetric structures with two mode I cracks of length a_1 and a_2. The initial state is $a_1 = a_2 = a_0$, with the stress intensity factors $K_1 = K_2 = K_c$ where K_c is the effective fracture toughness of the material. Now, the structure can exhibit three different equilibrium paths. For the case of linear fracture mechanics, these paths are characterized as follows:

$$\text{Path 1 (main): } \delta a_1 = \delta a_2 > 0 \quad \text{and} \quad \delta K_1 = \delta K_2 = 0, \tag{15}$$

$$\text{Path 2 (secondary): } \delta a_1 > 0, \quad \delta a_2 = 0 \quad \text{and} \quad \delta K_1 = 0, \quad \delta K_2 < 0, \tag{16}$$

$$\text{Path 3 (unloading): } \delta a_1 = \delta a_2 = 0 \quad \text{and} \quad \delta K_1 = \delta K_2 < 0. \tag{17}$$

There also exists the path $\delta K_1 < 0$, $\delta K_2 = 0$, which is, however, equivalent to path 2 because of symmetry. The inequalities in (15)–(17) represent the conditions of admissibility. The main path is always admissible for symmetric configurations, while the secondary path may be inadmissible in certain cases when the condition $\delta K_2 < 0$ (16) is violated for $\delta a_1 > 0$, in other words, the stress intensity factor at the stationary crack tip is increasing as the other crack is growing. Path 3 represents a trivial elastic equilibrium solution that does not require any fracture analysis; in the load-displacement diagram, path 3 is a straight line from the current state towards the origin.

4. *R*-curve and calculation of load-displacement curves

Based on linear elastic fracture mechanics, the mode I stress intensity factor of crack j ($j = 1, 2$) can be expressed as:

$$K_j = \sigma \sqrt{w} f_j(\alpha), \qquad \alpha = (a_1 + a_2)/w, \tag{18}$$

where $f_j(\alpha)$ is a nondimensional function which depends on the geometry of the specimen and the crack path. For path 1 (main), $f_1(\alpha) = f_2(\alpha) = f^m(\alpha)$ however, for path 2 (secondary) we have $f_1(\alpha) = f_1^s(\alpha)$ and $f_2(\alpha) = f_2^s(\alpha)$.

The material is assumed to have an R-curve behavior which depends on the specimen geometry and is based on the size effect analysis. The R-curve may be calculated as follows [9]:

$$\frac{R(c)}{G_f} = \frac{g'(\gamma)}{g'(\alpha_0)} \frac{c}{c_f} \tag{19}$$

in which

$$\frac{c}{c_f} = \frac{g'(\alpha_0)}{g(\alpha_0)} \left(\frac{g(\gamma)}{g'(\gamma)} - \gamma + \alpha_0 \right), \qquad \gamma = \alpha_0 + \alpha_c \tag{20}$$

$\alpha_0 = 2a_0/w$, $\alpha_c = c/w$, c = total crack extension for both cracks, $g(\gamma) = f_j^2(\gamma)$, and $g'(\gamma) = dg(\gamma)/d\gamma$; G_f = fracture energy and c_f = effective size of the fracture process zone. G_f and c_f are material properties defined for the limiting case of an infinitely large specimen.

The load required for crack propagation may be characterized by the nominal stress, which can be calculated from (18):

$$\sigma_N = \frac{K_c}{\sqrt{w} f_j(\alpha)}, \tag{21}$$

where K_c = effective fracture toughness = $[ER(c)]^{1/2}$, E = modulus of elasticity. Denoting $K_f = [EG_f]^{1/2}$ = fracture toughness, we can write

$$K_c = K_f \left(\frac{R(c)}{G_f} \right)^{1/2}. \tag{22}$$

It is convenient to define the nondimensional stress at crack propagation as follows:

$$s = \frac{\sqrt{w}}{K_f} \sigma_N = \frac{1}{f_j(\alpha)} \left(\frac{R(c)}{G_f} \right)^{1/2}. \tag{23}$$

For the case of linear elastic fracture mechanics we have $R(c) = G_f$, thus, $s = 1/f_j(\alpha)$. It is important to use the proper $f_j(\alpha)$ in the calculations; $f_j(\alpha) = f^m(\alpha)$ for path 1 and $f_j(\alpha) = f_1^s(\alpha)$ for path 2.

It is also convenient to define the nondimensional displacement, q, in terms of a characteristic displacement v:

$$q = \frac{E}{K_f \sqrt{w}} v. \tag{24}$$

If finite elements analysis is carried out to calculate functions $f_j(\alpha)$ at discrete values of α, then scaling the $f_j(\alpha)$ value by a factor according to (21) gives the nominal stress for pro-

pagation, σ_N, and v is obtained easily from the calculated nodal displacement values corresponding to σ_N.

In the case where $f_j(\alpha)$ is available as a continuous function and the load-point displacement is selected as the characteristic displacement, the value of v can be evaluated from the strain energy due to the crack:

$$U_c = \int_{\alpha}^{\alpha+\Delta\alpha} \frac{K_c^2}{E} w \, d\alpha = \frac{1}{E} \sigma_N^2 w^2 F(\alpha), \quad \text{where} \quad F(\alpha) = \int_{\alpha}^{\alpha+\Delta\alpha} f_j^2(\alpha) \, d\alpha. \tag{25}$$

The load-point displacement due to the crack can then be calculated according to Castigliano's theorem:

$$v_c = \frac{1}{2}\left(\frac{1}{w}\frac{\partial U_c}{\partial \sigma_N}\right) = \frac{\sigma_N}{E} w F(\alpha). \tag{26}$$

The total displacement v can then be calculated as:

$$v = v_b + v_c = \frac{\sigma_N}{E} w \left[\frac{1}{2}\frac{L}{w} + F(\alpha)\right], \tag{27}$$

where v_b is the load-point displacement of the body with no cracks present. Finally q is given by:

$$q = q_b + q_c = s\left[\frac{1}{2}\frac{L}{w} + F(\alpha)\right]. \tag{28}$$

In the numerical calculation of the $s(q)$ curves, one chooses an increasing sequence of α_c-values. For each α_c, the corresponding γ value may be obtained from (20) by iterations; subsequently, $R(c)$ is computed from (19). Now, it is possible to calculate s from (23) and then q from (28). By this procedure it is possible to evaluate any snapback which might occur in the $s(q)$ curve.

5. Example 1: Edge-cracked tension specimen

Consider a rectangular plate of width w, and length $L = 3.67w$, which has rigid segments of length $0.15L$ at each end as shown in Fig. 1. The plate initially has two equal edge notches of length a_0 and is loaded by a point-displacement v. For this problem the stress intensity factor values for path 2 seem unavailable in the literature, so finite elements have been used to calculate functions $f_j(\alpha)$, see Appendix. To validate the use of finite elements, function $f^m(\alpha)$ obtained for path 1 may first be compared to that given in Murakami's handbook [10]. The comparison, shown in Fig. 2a demonstrates the accuracy of the finite element method for this case.

The next step is to investigate the possibility of bifurcation, i.e. the existence of path 2, at various values of α_0. Figure 2b shows curves $f_1^s(\alpha)$ and $f_2^s(\alpha)$ at $\alpha_0 = 0.125$, 0.333 and 0.542. It is found that $f_1^s(\alpha) > f_2^s(\alpha)$ and so the conditions in (16) are satisfied; hence path 2 is admissible.

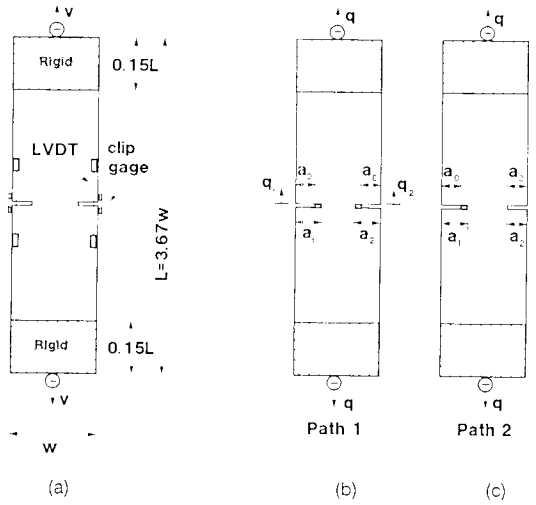

Fig. 1. (a) Edge-notched tension specimen with equal initial cracks; (b) Equilibrium path with both cracks growing (path 1); (c) Equilibrium path with one crack growing while the other remains stationary (path 2).

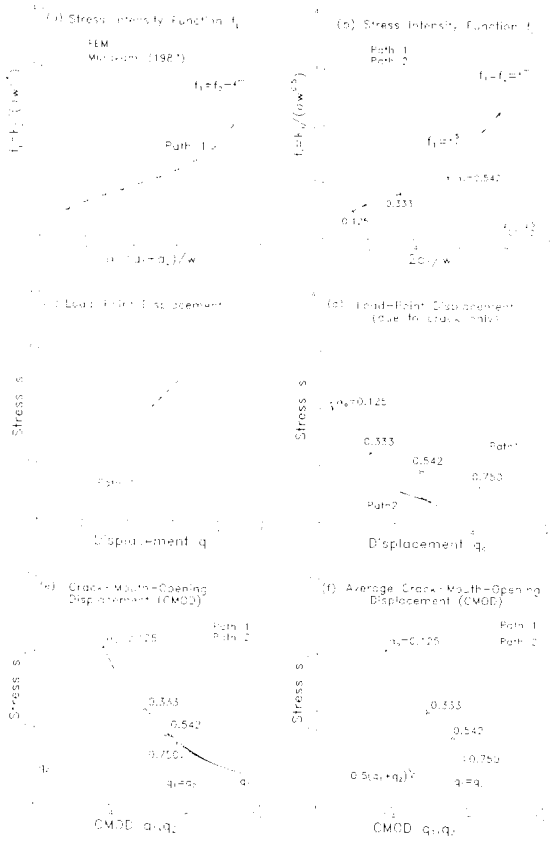

Fig. 2. (a) Stress intensity function for path 1 calculated from finite element analysis and compared to Murakami (1987); (b) Stress intensity functions for paths 1 and 2; (c) Stress versus total load-point displacement curve for path 1; Stress versus: (d) load-point displacement, (e) CMOD, and (f) average CMOD for path 1 with bifurcated paths 2 at $\alpha = 0.125$, 0.333, 0.542.

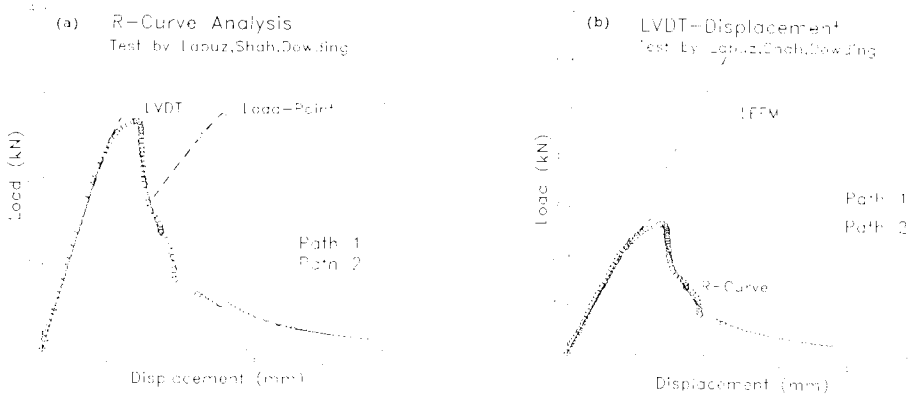

Fig. 3. (a) Load versus displacement (LVDT and Load-point) curves from *R*-curve analysis with data points from test results; (b) Load versus displacement (LVDT) curve from LEFM and *R*-curves analyses with data points from test results.

1. The fit of the LVDT-measured displacements is good for the full range of displacements reported, provided one uses path 2 in the analysis. If one uses path 1 it is possible to get a good fit up to the peak load only;
2. due to snapback in the curve of the load versus load-point displacement, this test specimen would have failed near the peak load if the load-point displacements were controlled instead of CMOD;
3. the LEFM analysis gives the same peak load for both paths 1 and 2, however from the *R*-curve analysis the peak load for path 2 is lower than that for path 1;
4. the LEFM solution for post-peak path 2 fits the experimental data at later stages of loading after the load is reduced to less than half the peak value.

The fact that crack growth in this kind of specimen is asymmetric has recently been reported by Rots, Hordijk and de Borst [12] who studied by finite elements the evolution of crack bands rather than line cracks. This conclusion is also in agreement with the experimental results of Cornelissen, Hordijk and Reinhardt [13] on tensile concrete specimens. Furthermore, it is interesting to note that measurements by Raiss, Dougill and Newman [14] on unnotched direct tension concrete specimens reveal similar behavior, in which the microcracking and fracture growth tend to localize to one side of the specimen.

6. Example 2: Centre-cracked tension strip

Consider a strip of width w, unit thickness and infinite length which initially contains a centric crack of length $2a_0$ in the transverse direction, and is loaded by uniform uniaxial stress s as shown in Fig. 4. The stress intensity factors for both symmetric and asymmetric crack growth are given for this problem in [10]. The curves of nondimensional nominal stress s versus nondimensional load-point displacement due to fracture q_c for paths 1 and 2 are shown in Fig. 4. The stable path is that which starts with bifurcation at the initial state ($\alpha_0 = 0.10$) of the symmetric path. This is because the tangential stiffness for path 2 is less than that for path 1 [8].

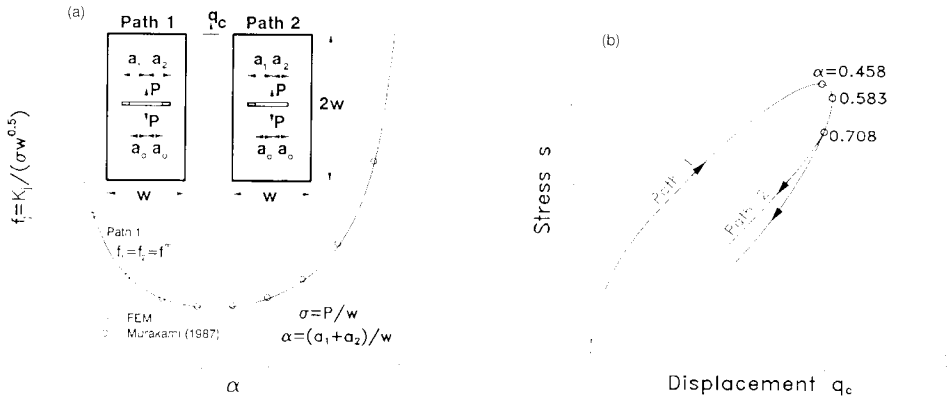

Fig. 5. (a) Stress intensity function for path 1 calculated from finite element analysis and compared to Murakami (1987); (b) Stress versus displacement (due to crack only) for a center-cracked plate loaded with a concentrated force P at the crack.

8. Example 4: Parallel equidistant cracks in a halfspace

Consider a homogeneous isotropic elastic halfspace in which a system of parallel equidistant cracks normal to the surface is produced by thermal stresses from cooling or by drying shrinkage (Fig. 6a). This problem arises in many applications. It was studied in detail with respect to a proposed hot-dry-rock geothermal energy scheme by Bažant et al. [16–18]; Nemat-Nasser, Keer and Parihar [19]; and Keer, Nemat-Nasser and Oranratnachai [20]. In this scheme, a large primary crack is created by hydraulic fracturing, by forcing water under high pressure into a bore several kilometers deep. Heat is extracted from the rock by circulating water through the crack. However, after a layer of rock at the surface of the crack walls cools down, the rate of heat conduction from the rock mass to the crack surface decreases, and thus the scheme can be viable only if further cracks, normal to the crack walls, can be produced by the cooling water. Another application is the shrinkage cracking of concrete, where the spacing of the open cracks is important because it determines the crack widths.

An interesting question is whether the bifurcation is stable or represents the limit of stable states. In the present thermal stress problem we have no prescribed displacements, however the penetration depth of cooling D can be substituted for q_j. Therefore, (4) reduces to

$$\sum_{r=1}^{m} \Phi_{rk}\delta a_r + \frac{\partial^2 \Pi}{\partial D \partial a_k}\delta D = 0, \tag{29}$$

where Φ_{rk} is given by (3) and D can be regarded as the controlled parameter. Let us first examine the bifurcation at the limit of stable states, at which there must be neutral equilibrium, i.e. (29) can be satisfied with nonzero δa_r at no change in temperature ($\delta D = 0$):

$$\sum_{r=1}^{m} \Phi_{rk}\delta a_r = 0. \tag{30}$$

Now consider bifurcation of the loading path at advancing cooling front, $\delta D > 0$. Equation (29) must be satisfied along each post-bifurcation branch, i.e.

$$\sum_{r=1}^{m} \Phi_{rk} \delta a_r^{(1)} + \frac{\partial^2 \Pi}{\partial D \partial a_k} \delta D = 0, \tag{31}$$

$$\sum_{r=1}^{m} \Phi_{rk} \delta a_r^{(2)} + \frac{\partial^2 \Pi}{\partial D \partial a_k} \delta D = 0, \tag{32}$$

in which the superscripts $^{(1)}$ and $^{(2)}$ refer to the post-bifurcation paths 1 and 2. Subtracting these equations, we get the conditions

$$\sum_{r=1}^{m} \Phi_{rk} \delta a_r^* = 0, \quad \text{with} \quad \delta a_r^* = \delta a_r^{(1)} - \delta a_r^{(2)}. \tag{33}$$

If there is bifurcation, δa_r^* must be nonzero, and so matrix $[\Phi_{rk}]$ must be singular, i.e. $\det[\Phi_{rk}] = 0$.

Numerical results obtained by finite elements indicate that the singularity of $[\Phi_{rk}]$ is achieved before the stability limit is reached. Therefore, the first bifurcation occurs in a stable manner during an advance of the cooling front, without any instability or neutral equilibrium. From (33) for $k = 1$:

$$\Phi_{11} \delta a_1^* + \Phi_{21} \delta a_2^* = 0. \tag{34}$$

Since $\Phi_{11} = \Phi_{21}$, we find $\delta a_1^* = -\delta a_2^*$, which means that $\delta a_1^{(1)} - \delta a_1^{(2)} = -(\delta a_2^{(1)} - \delta a_2^{(2)})$. Now for the main path we have $\delta a_1^{(1)} = \delta a_2^{(1)}$, which yields $\delta a_1^{(2)} + \delta a_2^{(2)} = 2\delta a_1^{(1)}$. Since the stress intensity factor of cracks a_2 for the secondary path is decreasing, we have $\delta a_2^{(2)} = 0$. Thus $\delta a_1^{(2)} = 2\delta a_1^{(1)}$, from which we finally conclude that:

$$\frac{1}{2} \frac{\partial a_1^{(2)}}{\partial D} = \frac{\partial a_1^{(1)}}{\partial D} = \frac{\partial a_2^{(1)}}{\partial D}. \tag{35}$$

This gives the direction of the secondary path as shown in Fig. 6b at point B.

It is interesting to note that the behavior in Fig. 6a is completely analogous to buckling of elasto-plastic columns. The bifurcation (point B) at increasing D, $\delta D > 0$, is analogous to the bifurcation at Shanley's tangent modulus load, which happens at increasing load and is stable, same as here. The critical state (point C) of the crack system at $\delta D = 0$ is analogous to Engesser-von Kármán's reduced modulus (double modulus) load of column at which neutral equilibrium occurs, the same as here. Finite element calculations show that the distance between points B and C (Fig. 6e) becomes smaller as the toughness of the material is increased.

9. Conclusions

1. The present formulation makes it possible to calculate the response paths and the tangential stiffness matrix of elastic structures with propagating cracks. Based on the tangential stiffness matrix, stability and bifurcations of the loading path can be analyzed.

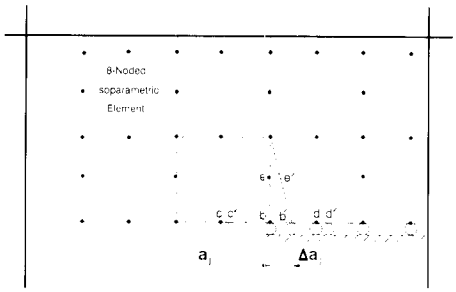

Fig. 7. Finite element mesh close to tip of crack a_j.

Calculation of K_j requires running the finite element program twice; for $a_j + \Delta a_j$ and $a_j - \Delta a_j$. Furthermore, $(-\Delta U)$ should be used instead of (ΔU) in (36) for the cases where the boundary conditions are prescribed displacements.

Surface $\delta^2 W_c$ for the specimen shown in Fig. 8

It is instructive to consider the surface of $\delta^2 W_c$, which represents the part of $\delta^2 W$ that is due to crack propagation [21]. Figure 9 shows the variation of $\delta^2 W_c$ as a function of $\delta u/w$ and $\delta\vartheta$, where δu = average axial displacement variation due to crack extension and $\delta\vartheta$ = rotation variation due to crack extension. Denoting δm and δf as the corresponding moment and force variations for $\delta\vartheta$ and δu respectively, we therefore have:

$$\delta^2 W_c = 0.5(\delta m\ \delta\vartheta + \delta f\ \delta u). \tag{37}$$

Figure 9 shows three surfaces corresponding to the initial states: $\alpha_0 = 0.20$, 0.44 and 0.76. The state with $\alpha_0 = 0.44$ is the critical state since under axial displacement control ($\delta u = 0$) the value of $\delta^2 W_c$ is 0. Furthermore, for $\alpha_0 = 0.20$ the state is stable ($\delta^2 W_c > 0$) and for $\alpha_0 = 0.76$ the state is unstable ($\delta^2 W_c < 0$). For each surface, the equilibrium paths for $\delta m = 0$ are labeled as 1, 2 and 3; these paths are also shown on the $s(q_c)$ curve in Fig. 8.

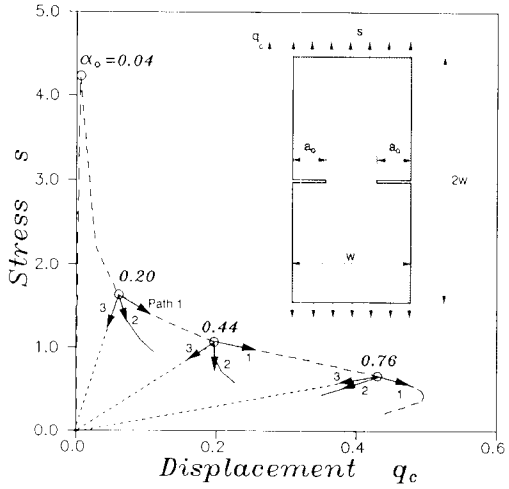

Fig. 8. Stress versus displacement curves of equilibrium paths 1, 2 and 3 for a specimen with equal initial edge cracks loaded by a uniform stress.

12. J.G. Rots, D.A. Hordijk and R. De Borst, in *Numerical Methods in Fracture Mechanics*, A.R. Luxmoore et al. (eds.), Pineridge Press, Swansea (1987) 457–471.
13. H.A. Cornelissen, D.A. Hordijk and H.W. Reinhardt, *HERON* 31, No. 2 (1986) 45–56.
14. M.E. Raiss, J.W. Dougill and J.B. Newman, in *Fracture of Concrete and Rock: Recent Developments*, S.P. Shah, S.E. Swartz and B. Barr (eds.), Elsevier, London (1989) 243–253.
15. A. Alvarado, S.P. Shah and R. John, *Journal of Engineering Mechanics*, ASCE 115, No. 2 (1989) 366–383.
16. Z.P. Bažant and H. Ohtsubo, *Mechanics Research Communication* 4, No. 5 (1977) 353–366.
17. Z.P. Bažant, H. Ohtsubo and K. Aoh, *International Journal of Fracture* 15, No. 5 (1979) 443–456.
18. Z.P. Bažant and A. Wahab, *Journal of Engineering Mechanics*, ASCE 105, EM5 (1979) 873–889.
19. S. Nemat-Nasser, L.M. Keer and K.S. Parihar, *International Journal of Solids and Structures* 14 (1978) 409–430.
20. L.M. Keer, S. Nemat-Nasser and A. Oranratnachai, *International Journal of Solids and Structures* 15 (1979) 111–126.
21. Z.P. Bažant, M.R. Tabbara and M.T. Kazemi, in *Proceedings of the Seventh International Conference on Fracture (ICF7)*, Houston, Texas (1989) 2141–2152.
22. Z.P. Bažant and L. Cedolin, *Stability of Structures: Elastic, Inelastic, Fracture and Damage Theories*, Oxford University Press, New York (1991).

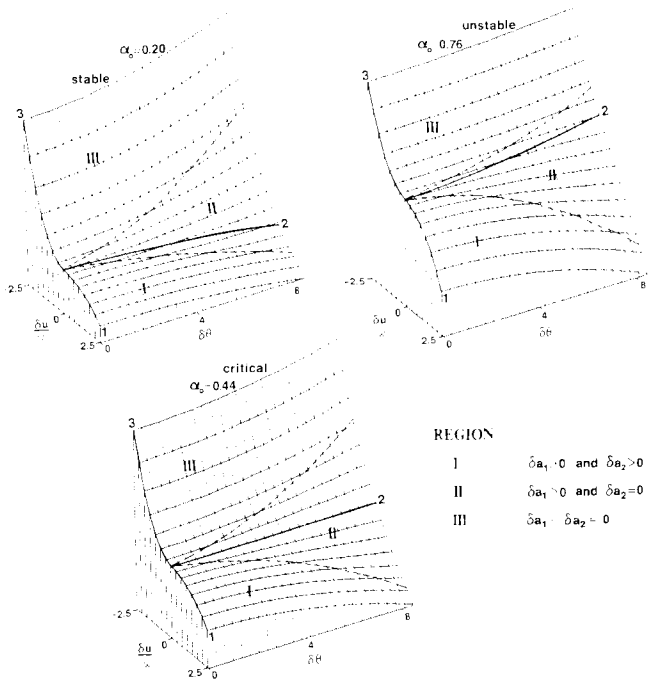

Fig. 9. Surfaces of second order work due to crack extension for the specimen shown in Fig. 8.

Acknowledgement

The general theory was supported under AFOSR Contract F49620-87-C-0030DEF with Northwestern University and the stability analysis of fracture specimens was supported by the NSF Center for Advanced Cement-Based Materials at Northwestern University.

References

1. G. Meier, *International Journal of Solids and Structures* 7 (1971) 345–372.
2. Z.P. Bažant, *Journal of Engineering Mechanics*, ASCE 102, EM2 (1976) 331–344.
3. H. Petryk, in *Plasticity Today: Modeling, Methods and Applications*, A. Sawczuk and G. Bianchi (eds.), Elsevier, London (1985) 429–447.
4. Q.S. Nguyen and C. Stolz, in *IUTAM Symposium on Application of Multiple Scaling in Mechanics*, E.N.S., Paris, France (1986).
5. Q.S. Nguyen, *Journal of Mechanics and Physics of Solids* 35, No. 3 (1987) 303–324.
6. C. Stolz, in *Proceedings of France–U.S. Workshop on Strain Localization and Size Effect due to Cracking and Damage*, J. Mazars and Z.P. Bažant (eds.), E.N.S., Cachan, France (1988) 207–216.
7. R. Hill, *Journal of the Mechanics and Physics of Solids* 6 (1958) 236–249.
8. Z.P. Bažant, *Journal of Engineering Mechanics*, ASCE 114, No. 12 (1988) 2013–2034.
9. Z.P. Bažant and M.T. Kazemi, Report 88-7/498d, Center for Concrete and Geomaterials, Northwestern University, Evanston, Illinois (1988), also *International Journal of Fracture* 44 (1990) 111–131.
10. Y. Murakami, *Stress Intensity Factors Handbook*, Pergamon Press (1987).
11. J.F. Labuz, S.P. Shah and C.H. Dowding, in *Proceedings of ASCE Symposium*, C.H. Dowding (ed.), Denver, Colorado (1985) 158–163.

2. The existing finite element programs for fracture generally do not carry out checks for the development of asymmetric response in symmetric structures, as here. Such programs yield symmetric solutions for the present edge-cracked tensile specimen, which is incorrect.
3. For various typical crack configurations considered in practice and listed in textbooks and handbooks, it is found that symmetric crack propagation is not the stable path. Rather, the stable path involves a breakdown of symmetry, due to asymmetric propagation of the crack system.
4. *R*-curve behavior of the material significantly alters the response, but bifurcation stability problems occur again, and normally the breakdown of symmetry, with asymmetric crack propagation, represents the correct (stable) response path.
5. For the problem of growth of a system of parallel equidistant cooling or shrinkage cracks in a halfspace, the solution confirms the previous findings that (1) there is a critical state at the limit of stability (with neutral equilibrium), at which every other crack suddenly jumps ahead and the remaining cracks unload, and that (2) there is a stable bifurcation that precedes the stability limit. At the first bifurcation there is no neutral equilibrium and the response is stable, every other crack growing gradually with the progress of cooling and the remaining cracks gradually unloading. The first bifurcation is analogous to Shanley's bifurcation at the tangent modulus load of elastic-plastic column, while the critical state of stability limit of the crack system is analogous to the Engesser-von Kármán reduced modulus load.

Remark

It is widely thought that the finite element solutions are correct if the iterations of the loading step converge. This is not true, however. The convergence of iterations depends only on the stability of state, and has nothing to do with stability of path. The symmetric solution is an unstable path, yet it consists of stable states.

Appendix

Calculation of stress intensity factors

For the cases where the mode I stress intensity factors are not available in the literature, it is possible to use the finite element method to get a good estimate of K_j by:

$$K_j = \left(\frac{\Delta U}{2\Delta a_j} E'\right)^{1/2}, \tag{36}$$

where $\Delta U = U(a_j + \Delta a_j) - U(a_j - \Delta a_j)$ and Δa_j = small increment in a_j, $E' = E$ for plane stress, $E' = E/(1 - \nu^2)$ for plane strain, E = modulus of elasticity, ν = Poisson's ratio.

Figure 7 shows part of the finite element mesh close to the tip of crack a_j. The increment in a_j is achieved by moving the four nodes (b, c, d, e) to (b', c', d', e'); node b at the crack tip, is moved by a distance Δa_j, while nodes (c, d, e) are moved by a distance $(\Delta a_j)/2$.

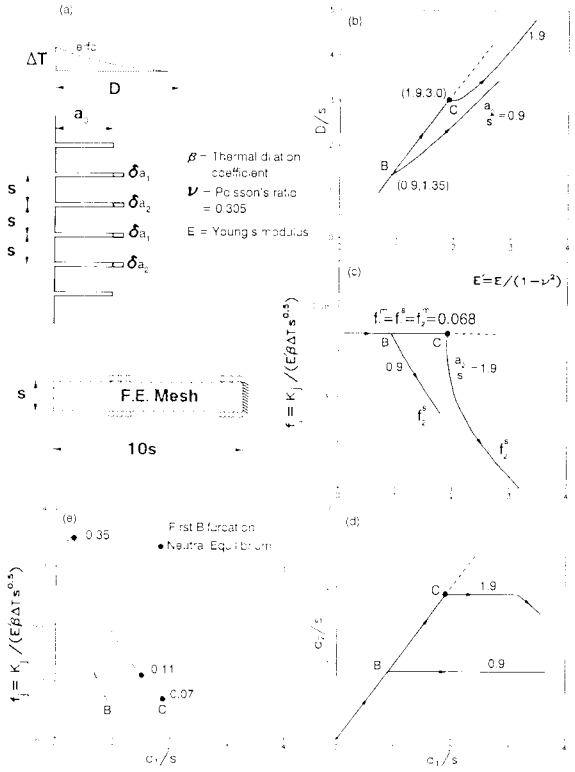

Fig. 6. (a) Halfspace with a system of parallel equidistant initial cracks loaded with a temperature ΔT at the surface; (b) Penetration depth versus crack length curves with the point of first bifurcation B and the point of critical equilibrium C; (c) Nondimensional stress intensity factors for paths 1 and 2 as they vary with increasing crack length; (d) Crack length plot for paths 1 and 2; (e) Distance BC, between first bifurcation point and neutral equilibrium point, as it varies with material toughness.

One simple possibility is that every other crack extends, $\delta a_1 > 0$, while the intermediate cracks remain stationary, $\delta a_2 = 0$ (Fig. 6a). Then we have $m = 1$ ($M = 2$), and $\det[\Phi_{rk}] = \Phi_{11}$. Assuming the material to obey linear elastic fracture mechanics, we further have $\Phi_{11} = \partial^2 \Pi / \partial a_1^2$. Since $\delta^2 W = \frac{1}{2}\Phi_{11}\delta a_1^2$ (14), the state is stable if $\Phi_{11} > 0$, unstable if $\Phi_{11} < 0$, and critical if $\Phi_{11} = 0$, as shown previously [16, 19]. In terms of the stress intensity factor, the critical state condition is that the derivative $\partial K_1/\partial a_1 = 0$ at constant a_2. The associated instability mode consists of an advance of every other crack by $\delta a_1 > 0$, occurring at $\delta a_2 = 0$ and at constant D. This instability mode can be correct only if K_2 does not increase during instability. Indeed, numerical solutions show that K_2 decreases during instability, i.e. the arrested, stationary cracks cease to be critical, while of course K_1 remains equal to fracture toughness K_c (Fig. 6c).

It remains to be examined whether bifurcation instability can occur at constant D with both δa_1 and δa_2 being nonzero ($m = M = 2$). Previous works [16, 17, 19] showed this to be impossible because the corresponding instability mode (eigenvector) δa_r violates the condition that $\delta a_2 \geqslant 0$.

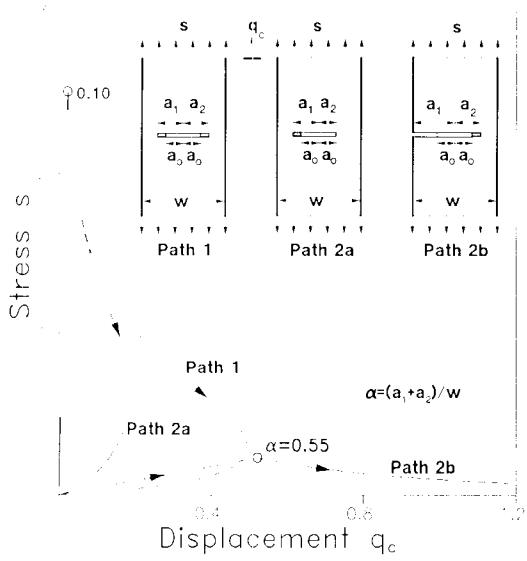

Fig. 4. Stress versus displacement (due to crack only) curves for a center-cracked strip loaded with a far-field stress s.

The calculations according to linear elastic fracture mechanics show that, under displacement control, the crack can grow in a stable equilibrium manner only towards one side. It grows until snapback instability is reached, after which the crack propagation becomes dynamic, the ligament on one side is completely ruptured and what remains is a single crack extending all the way to the edge. During further displacement increase, this crack later becomes critical at $\alpha = 0.55$, after which the fracture is completed by the growth of this single crack towards the opposite edge.

7. Example 3: Centre-cracked specimen loaded on the crack

A different behavior is encountered for a rectangular specimen with a centric crack which is loaded by a pair of concentrated forces at the middle of the crack surfaces, as shown in Fig. 5a. The $s(q_c)$ curves are calculated from linear elastic fracture mechanics. First we note that, in contrast to the curves in Figs. 2d and 4, the stress-displacement curve initially rises up to a peak at $\alpha = 0.458$. Furthermore, the secondary path is not admissible for $\alpha \leqslant 0.708$ because it violates the admissibility condition in (16). So in this case the propagation is symmetric up to $\alpha = 0.583$ after which the specimen fails due to snap-back instability. This seems to agree with experimental observations of Alvarado, Shah, and John [15] on failure crack patterns of similar specimens. In this case the values of $f_j(\alpha)$ were evaluated from finite element analysis. To examine the accuracy of this analysis for this case, it is necessary to compare function $f^m(\alpha)$ obtained for path 1 with that given in [10]. This is done in Fig. 5a which shows good agreement and validates the use of the finite element method for calculating the $f_j(\alpha)$ functions.

In this example we consider three nondimensional displacements; q = load-point displacement, q_1 = CMOD (crack mouth opening displacement) of crack 1 and q_2 = CMOD of crack 2. We have $q_1 = q_2$ for path 1 and $q_1 > q_2$ for path 2.

The surface $\delta^2 W$ for this type of specimen is illustrated and discussed in the Appendix.

5.1. *Cracks obeying linear elastic fracture mechanics*

The nondimensional stress-displacement curve $s(q)$ for path 1 is shown in Fig. 2c. All the states on this path are unstable under q-control because a snapback path exists at each state. Under q_1 control (Fig. 2e), on the other hand, path 1 shows no snapback for $\alpha_0 \leqslant 0.750$. Next we investigate stability of the states at points on path 1. For this we need to calculate the tangential stiffness matrix $[S_{ij}^t]$ as given by (9), which is a 3×3 matrix in this case. Stability of state requires that $[S_{ij}^t]$ be positive definite under the constraint $\delta q_1 = 0$ (q_1-control), this condition is satisfied for $\alpha_0 = 0.125$, 0.333 and 0.542. Now, consider path bifurcation at stable states of path 1. The bifurcated path (path 2), shown in Fig. 2e at the three values of α_0, has two branches q_1 and q_2. The q_1-branch exhibits no snapback. So, for a positive increment in q_1, we have two possible equilibrium paths. But since the structure can follow just one path it is necessary to decide between path 1 and path 2. The $s(q_c)$ curves for paths 1 and 2 are shown in Fig. 2d; the stable path is the one with the lower stiffness [8], which is found to be path 2 in this case.

One more type of control is of interest; namely controlling the average CMOD, i.e. $q_a = 0.5(q_1 + q_2)$. This type of control has no effect on path 1, and so the same curve as in Fig. 2e is shown in Fig. 2f. To investigate stability of the states at points on path 1, we consider the same $[S_{ij}^t]$ as before but under the constraint $\delta q_a = 0$. Calculations show that the states on path 1 are also stable under q_a-control. Now, examining the curves for path 2, we see that snapback exists at all three points. So, for a positive increment in q_a, the structure snaps vertically down (in a dynamic manner) to the next available equilibrium state on path 2.

5.2. *Cracks with R-curve behavior*

The foregoing results cannot be experimentally verified on test specimens of materials such as concrete, rock or ceramics because these materials exhibit pronounced R-curve behavior, i.e. the energy required for crack propagation is not constant but varies as a function of the effective crack length. So the introduction of an R-curve in the calculations is necessary for comparison with test data. The specimen in Fig. 1 was actually conceived to model the test specimens of Labuz, Shah, and Dowding [11]. The experiments were conducted under average CMOD control which was provided by two clip gages mounted as shown in Fig. 1. The load-line displacements were measured with two LVDT displacement transducers mounted on the face of these specimens across the notches, and the average of these two displacements was recorded. The acoustic emission method had been used for micro-crack location, which revealed that crack growth was asymmetric, even though care had been taken to produce symmetric crack propagation.

The load-displacement curves for paths 1 and 2 shown in Fig. 3 were calculated using the following material parameters: $E = 47.6$ GPa, $G_f = 0.165$ N/m and $c_f = 27.9$ mm. These parameters were evaluated by fitting the experimentally obtained results which are represented by the data points in Fig. 3. Several observations can be made: